A first-order *k*-space model for elastic wave propagation in heterogeneous media

K. Firouzi[a)]
Department of Mechanical Engineering, University College London, London, WC1E 7JE, United Kingdom

B. T. Cox
Department of Medical Physics and Bioengineering, University College London, London, WC1E 6BT, United Kingdom

B. E. Treeby
College of Engineering and Computer Science, Australian National University, Canberra, Australian Capital Territory 0200, Australia

N. Saffari
Department of Mechanical Engineering, University College London, London, WC1E 7JE, United Kingdom

(Received 20 September 2011; revised 31 May 2012; accepted 1 June 2012)

A pseudospectral model of linear elastic wave propagation is described based on the first order stress-velocity equations of elastodynamics. *k*-space adjustments to the spectral gradient calculations are derived from the dyadic Green's function solution to the second-order elastic wave equation and used to (a) ensure the solution is exact for homogeneous wave propagation for timesteps of arbitrarily large size, and (b) also allows larger time steps without loss of accuracy in heterogeneous media. The formulation in *k*-space allows the wavefield to be split easily into compressional and shear parts. A perfectly matched layer (PML) absorbing boundary condition was developed to effectively impose a radiation condition on the wavefield. The staggered grid, which is essential for accurate simulations, is described, along with other practical details of the implementation. The model is verified through comparison with exact solutions for canonical examples and further examples are given to show the efficiency of the method for practical problems. The efficiency of the model is by virtue of the reduced point-per-wavelength requirement, the use of the fast Fourier transform (FFT) to calculate the gradients in *k* space, and larger time steps made possible by the *k*-space adjustments. © *2012 Acoustical Society of America*. [http://dx.doi.org/10.1121/1.4730897]

PACS number(s): 43.20.Gp, 43.20.Bi, 43.35.Cg, 43.20.Px [TDM] Pages: 1271–1283

I. INTRODUCTION

Numerical models of elastic wave propagation are used in many different fields, including seismology, geophysics and soil mechanics,[1,2] non-destructive testing,[3] condensed matter physics,[4] design of SAW devices and other types of sensor and transducer,[5,6] and biomedical ultrasound.[7] A number of different numerical methods have been used to solve the elastic wave equations but among the more commonly used are finite elements,[8] boundary elements,[9] finite volume,[10,11] integral equations,[12] finite-differences,[13–15] or pseudospectral models.[16–18] This paper describes a model of elastic wave propagation in isotropic, heterogeneous solid media using a *k*-space method, a variation on the pseudospectral theme.

Spectral methods are characterized by the use of Fourier or polynomial basis functions to describe the field variables and have the advantages over finite difference methods that the mesh requirements are more relaxed, requiring only two nodes per wavelengths, and that the spatial gradients can in many cases (such as Fourier collocation) be calculated efficiently using fast Fourier transforms.[19–21] *Pseudo*spectral models are spectral models for which the time derivatives are calculated using finite differences.[22] *k*-space methods also use a spectral approach to calculate the derivatives but look for ways to improve the approximation of the temporal derivative. *k*-space methods are typically used for hyperbolic problems for which an exact solution is known in the homogeneous case. In some cases this allows an adjustment to be made to either the (finite difference) time derivative or the (spectral) spatial derivatives which converts the time-stepping pseudospectral model into an exact model for homogeneous media, and stable for larger timesteps (for a given level of accuracy) in heterogeneous media. An early use of a *k*-space adjustment to a gradient calculation to improve a pseudospectral method was made by Fornberg and Whitham,[23] who applied it to a nonlinear wave equation, but did not use the term "*k*-space." Bojarski and others[24–29] applied similar ideas to linear scalar wave equations, with clear applications in acoustics and ultrasound, but Liu[30] was the first to apply *k*-space ideas to elastic wave problems. He derived a *k*-space form of the dyadic Green's function for the elastic wave equation and used it, in conjunction with equivalent source terms accounting for medium heterogeneities, to calculate the scattered field iteratively in a Born

[a)]Author to whom correspondence should be addressed. Electronic mail: kamyar.firouzi.09@ucl.ac.uk

series. In a slightly different approach, Tabei *et al.*[31] proposed a *k*-space method for solving a pair of coupled first order acoustic equations, rather than a second order wave equation, which has been applied to scalar acoustic problems.[32,33] This paper extends their approach to the elastic wave case. The principal differences of this method over that of Liu[30] are that due to the fact that we solve first order equations rather than a second order wave equation. This allows velocity (or displacement) as well as stress sources to be implemented simply, and permits the straightforward inclusion of a perfectly matched layer (PML) as an absorbing boundary. The implementation of the PML used here, however, requires each of the field variables to be split into three directions which will increase the overall memory requirements.

The layout of this paper is as follows. The *k*-space model of elastic wave propagation is derived in Sec. II. More specifically, in Sec. II A. the equations used to model elastic waves are briefly reviewed, in Sec. II B an exact *k*-space solution of the elastic wave equations is derived, this solution is compared to a leapfrog pseudo-spectral method in order to derive two *k*-space propagators corresponding to compressional and shear wave propagation in Sec. II C, and in Sec. II D their use in a model based on the first order elastic wave equations is considered. Two characteristics of the model are the use of the dyadic wavenumber tensor to split the field into shear and compressional components, and the use of separate propagators for the shear and compressional components. The details of the numerical implementation, including the staggered grid, absorbing boundary conditions and source terms are described in Sec. III, examples and validating comparisons to analytical solutions are given in Sec. IV, and a discussion section and summary conclude the paper.

II. *k*-SPACE MODEL OF ELASTIC WAVE PROPAGATION

A. Governing equations

The fundamental equations used to describe deformation in isotropic elastic solids are the relationships between displacement u_i, strain ϵ_{ij}, and stress σ_{ij}:

$$\sigma_{ij} = \lambda\delta_{ij}\epsilon_{kk} + 2\mu\epsilon_{ij}, \tag{1}$$

$$\epsilon_{ij} = \frac{1}{2}\left(\frac{\partial u_i}{\partial x_j} + \frac{\partial u_j}{\partial x_i}\right), \tag{2}$$

where μ and λ are the Lamé elastic constants and are x_i, $i = 1, 2, 3$, Cartesian position coordinates. To model the propagation of lossless elastic waves it is enough to add Newton's second law:

$$\rho\frac{\partial^2 u_i}{\partial t^2} = \frac{\partial \sigma_{ij}}{\partial x_j} + f_i, \tag{3}$$

where f_i is a body force and ρ is the mass density. The Lamé constants are related to the propagation speeds of shear and compressional waves, c_s^2 and c_p^2, as

$$\mu = c_s^2\rho, \quad \lambda + 2\mu = c_p^2\rho. \tag{4}$$

Equations (1)–(3) can be written as two coupled first order equations

$$\frac{\partial \sigma_{ij}}{\partial t} = \lambda\delta_{ij}\frac{\partial v_k}{\partial x_k} + \mu\left(\frac{\partial v_i}{\partial x_j} + \frac{\partial v_j}{\partial x_i}\right), \tag{5}$$

$$\rho\frac{\partial v_i}{\partial t} = \frac{\partial \sigma_{ij}}{\partial x_j} + f_i, \tag{6}$$

where $v_i = \partial u_i/\partial t$ is the velocity vector. The numerical model described in this paper is based on these first-order equations. However, the *k*-space method is derived from the second order wave equation which can be obtained by eliminating the stress tensor from Eqs. (5) and (6). In vector notation with $\mathbf{u} = (u_1, u_2, u_3)$ it has the form (following some rearrangement):

$$\rho\frac{\partial^2 \mathbf{u}}{\partial t^2} = \nabla\lambda(\nabla\cdot\mathbf{u}) + \nabla\mu\cdot\left(\nabla\mathbf{u} + (\nabla\mathbf{u})^{\mathrm{T}}\right) + (\lambda + 2\mu)\nabla(\nabla\cdot\mathbf{u}) - \mu\nabla\times(\nabla\times\mathbf{u}) + \mathbf{f}, \tag{7}$$

where $\mathbf{f}$ is the vector force term. (We will move between the index and bold vector notation, and even combine them if necessary, to give the clearest expressions.) When the medium is homogeneous, so that the gradients of the Lamé parameters in the first two terms are zero, this reduces to the elastic wave equation

$$\frac{\partial^2 \mathbf{u}}{\partial t^2} - c_p^2\nabla(\nabla\cdot\mathbf{u}) + c_s^2\nabla\times(\nabla\times\mathbf{u}) = 0, \tag{8}$$

where the forcing term has been left out for simplicity. Note that when the coupled first order Eqs. (5) and (6) are solved numerically for a heterogeneous medium, it is equivalent to solving Eq. (7). However, the *k*-space method will be motivated by examining solutions in the homogeneous case, Eq. (8).

B. Exact *k*-space solution for a homogeneous medium

In Fourier spectral methods the wavefield is mapped from the spatial domain, $\mathbf{x} = (x_1, x_2, x_3)$, to the wavenumber domain or *k*-space, $\mathbf{k} = (k_1, k_2, k_3)$, using Fourier transforms, i.e. the wavefield is decomposed spatially into Fourier components:

$$\mathrm{u_j}(\mathbf{x}) = \sum_{\mathbf{k}} \mathrm{U_j}(\mathbf{k})e^{i\mathbf{k}\cdot\mathbf{x}}, \tag{9}$$

where $\mathbf{U} = (U_1(\mathbf{k}), U_2(\mathbf{k}), U_3(\mathbf{k}))$ is the displacement vector in *k*-space.

The spatial gradients can now be calculated straightforwardly as

$$\frac{\partial}{\partial x_j} = F^{-1}\{ik_jF\{\cdot\}\}, \tag{10}$$

where i is the imaginary unit. By writing the spatial gradient operator as $\nabla = i\mathbf{k}$ and recalling that

$$\mathbf{k}\times(\mathbf{k}\times\mathbf{U}) = (\mathbf{kk} - k^2\mathrm{I})\cdot\mathbf{U}, \tag{11}$$

where $\mathbf{kk}$ is the dyadic tensor formed by the outer product of $\mathbf{k}$ with itself, $k = |\mathbf{k}|$, and I is the identity matrix, Eq. (8) can be written in k-space as[12]

$$\frac{\partial^2\mathbf{U}}{\partial t^2} + k^2\left(c_p^2(\widehat{\mathbf{k}}\widehat{\mathbf{k}}) + c_s^2(\mathrm{I} - \widehat{\mathbf{k}}\widehat{\mathbf{k}})\right)\cdot\mathbf{U} = 0, \tag{12}$$

where $\widehat{\mathbf{k}} = \mathbf{k}/k$ is the unit vector in direction. $\mathbf{k}$ (Note that for a single frequency oscillation, for which the time derivative becomes $-\omega^2$, there is no simple dispersion relation between ω and k. This k does not have a simple physical interpretation, as it would if $c_s = 0$ or $c_p = 0$.)

As the medium is homogenous the compressional and shear waves will travel independently and they can therefore be separated. Formally, we write the displacement as the sum of scalar and vector potentials. In k-space this is

$$\mathbf{U} = \mathbf{U}_p + \mathbf{U}_s = i\mathbf{k}\phi + i\mathbf{k}\times\boldsymbol{\psi}, \tag{13}$$

where $\mathbf{U}_p = i\mathbf{k}\phi$ and $\mathbf{U}_s = i\mathbf{k}\times\boldsymbol{\psi}$ are the compressional and shear components of the displacement field. Substituting this into Eq. (12), and using the dyadic identities

$$\begin{aligned}&\widehat{\mathbf{k}}\widehat{\mathbf{k}}\cdot\mathbf{k} = \mathbf{k}, && (\mathrm{I} - \widehat{\mathbf{k}}\widehat{\mathbf{k}})\cdot\mathbf{k} = 0\\ &\widehat{\mathbf{k}}\widehat{\mathbf{k}}\cdot(\mathbf{k}\times\boldsymbol{\Phi}) = 0, && (\mathrm{I} - \widehat{\mathbf{k}}\widehat{\mathbf{k}})\cdot(\mathbf{k}\times\boldsymbol{\Phi}) = \mathbf{k}\times\boldsymbol{\Phi} \text{ for any } \boldsymbol{\Phi},\end{aligned} \tag{14}$$

allows Eq. (12) to be split into two parts corresponding to compressional and shear wave propagation

$$\left(\frac{\partial^2}{\partial t^2} + (c_p k)^2\right)\phi = 0, \tag{15}$$

$$\left(\frac{\partial^2}{\partial t^2} + (c_s k)^2\right)\boldsymbol{\psi} = 0. \tag{16}$$

These equations are satisfied by the scalar Green's functions

$$g_p(\mathbf{k},\mathrm{t}) = \begin{cases} 0, & t < 0\\ \sin(c_p k t)/(c_p k), & t \geq 0,\end{cases} \tag{17}$$

$$g_s(\mathbf{k},\mathrm{t}) = \begin{cases} 0, & t < 0\\ \sin(c_s k t)/(c_s k), & t \geq 0.\end{cases} \tag{18}$$

Using these solutions, a dyadic Green's function that satisfies Eq. (12) for a vector source term can be written as

$$G(\mathbf{k},\mathrm{t}) = G_p(\mathbf{k},\mathrm{t}) + G_s(\mathbf{k},\mathrm{t}), \tag{19}$$

where

$$G_p(\mathbf{k},\mathrm{t}) = \begin{cases} 0, & t < 0\\ \widehat{\mathbf{k}}\widehat{\mathbf{k}}\sin(c_p k t)/(c_p k), & t \geq 0,\end{cases} \tag{20}$$

$$G_s(\mathbf{k},\mathrm{t}) = \begin{cases} 0, & t < 0\\ (\mathrm{I} - \widehat{\mathbf{k}}\widehat{\mathbf{k}})\sin(c_s k t)/(c_s k), & t \geq 0.\end{cases} \tag{21}$$

The dyadic Green's function is required when the source (forcing) function is a vector. In this case the solution, in k-space, is

$$\mathbf{U}(\mathbf{k},\mathrm{t}) = \int G(\mathbf{k},\mathrm{t}-t')\cdot\mathbf{F}(\mathbf{k},t')dt'. \tag{22}$$

If the displacement is zero for $t < 0$, but abruptly becomes $\mathbf{U}_0(\mathbf{k})$ at $t = 0$, this is equivalent to a source term of the form $\mathbf{F} = \mathbf{U}_0\delta'(t)$ and the solution to this initial value problem becomes[30]

$$\mathbf{U}(\mathbf{k},\mathrm{t}) = \cos(c_p k t)\widehat{\mathbf{k}}\widehat{\mathbf{k}}\cdot\mathbf{U}_0 + \cos(c_s k t)(\mathrm{I} - \widehat{\mathbf{k}}\widehat{\mathbf{k}})\cdot\mathbf{U}_0. \tag{23}$$

C. Second-order model for a homogeneous medium: Shear and compressional *k*-space adjustments

A time-stepping pseudospectral formulation of Eq. (12) that uses a first order finite difference step in time can be written as

$$\frac{\mathbf{U}(\mathbf{k},t+\Delta t) - 2\mathbf{U}(\mathbf{k},t) + \mathbf{U}(\mathbf{k},t-\Delta t)}{\Delta t^2} = -k^2\left(c_p^2(\widehat{\mathbf{k}}\widehat{\mathbf{k}}) + c_s^2(\mathrm{I} - \widehat{\mathbf{k}}\widehat{\mathbf{k}})\right)\cdot\mathbf{U}. \tag{24}$$

Using the fact that $\mathbf{U}_p = i\mathbf{k}\phi$ so $\widehat{\mathbf{k}}\widehat{\mathbf{k}}\cdot\mathbf{U}_p = \mathbf{U}_p$ and $(\mathrm{I} - \widehat{\mathbf{k}}\widehat{\mathbf{k}})\cdot\mathbf{U}_p = 0$, and $\mathbf{U}_s = i\mathbf{k}\times\boldsymbol{\psi}$ so $\widehat{\mathbf{k}}\widehat{\mathbf{k}}\cdot\mathbf{U}_s = 0$ and $(\mathrm{I} - \widehat{\mathbf{k}}\widehat{\mathbf{k}})\cdot\mathbf{U}_s = \mathbf{U}_s$ [see Eqs. (14)] gives

$$\mathbf{U}(\mathbf{k},t+\Delta t) - 2\mathbf{U}(\mathbf{k},t) + \mathbf{U}(\mathbf{k},t-\Delta t) = -4\left(\frac{c_p k\Delta t}{2}\right)^2\mathbf{U}_p - 4\left(\frac{c_s k\Delta t}{2}\right)^2\mathbf{U}_s. \tag{25}$$

Now, by using the trigonometric identities $\cos\left(c_p k(t\pm\Delta t)\right) = \cos(c_p k t)\ \cos(c_p k\Delta t) \mp \sin(c_p k t)\sin\left(c_p k(t\pm\Delta t)\right)$ with Eq. (23) the following expression can be found:

$$\mathbf{U}(\mathbf{k},t+\Delta t) - 2\mathbf{U}(\mathbf{k},t) + \mathbf{U}(\mathbf{k},t-\Delta t) = -4\sin^2\left(\frac{c_p k\Delta t}{2}\right)\mathbf{U}_p(\mathbf{k},t) - 4\sin^2\left(\frac{c_s k\Delta t}{2}\right)\mathbf{U}_s(\mathbf{k},t). \tag{26}$$

This is a time-stepping solution to Eq. (12) which is exact for any size of time step Δt. Comparing this to Eq. (24), which is limited to small Δt, shows that by replacing $(c_{p,s}k\Delta t/2)^2$ with $\sin^2(c_{p,s}k\Delta t/2)$ it is possible to extend the length of the timestep which can be taken without reducing accuracy. This opens up two possibilities: (a) replacing Δt with $\Delta t\,\mathrm{sinc}(c_{p,s}k\Delta t/2)$ or (b) replacing k^2 with $k^2\mathrm{sinc}^2(c_{p,s}k\Delta t/2)$. As the k^2 arises from the gradient terms in Eq. (8) when writing $\nabla \to i\mathbf{k}$, an adjustment to this substitution which would result in Eq. (26) would be

$$\nabla_{p,s} \to i\mathbf{k}\,\mathrm{sinc}(c_{p,s}k\Delta t/2). \tag{27}$$

These k-space adjustments are used below for the calculation of the derivatives in a first order model.

D. First-order *k*-space model for a heterogeneous medium

One way to approach the case of propagation through a heterogeneous medium is to consider the perturbations in the medium properties as time-varying effective source terms in the *second order* wave equation. However, in order to be able to implement an absorbing boundary condition (ABC) that effectively imposes a radiation condition on the field by absorbing any *outward* travelling waves that reach the edge of the domain of interest it is convenient to work with the first order coupled equations, Eqs. (5) and (6). Such an ABC is necessary in Fourier based methods to avoid wave-wrapping (see Sec. III below). By replacing each temporal derivative with a forward finite difference approximation, these equations can be written in a way that allows them to be numerically integrated sequentially, one timestep Δt at a time [note that since in the heterogeneous case the material properties can be a function of space, the elastic constants and the density have an explicit $(\mathbf{r})$ dependence]:

$$\sigma_{ij}(\mathbf{r},t+\Delta t)=\sigma_{ij}(\mathbf{r},t)+\Delta t\lambda(\mathbf{r})\delta_{ij}\frac{\partial v_k(\mathbf{r},\mathrm{t})}{\partial x_k}+\Delta t\mu(\mathbf{r})\left(\frac{\partial v_i(\mathbf{r},\mathrm{t})}{\partial x_j}+\frac{\partial v_j(\mathbf{r},\mathrm{t})}{\partial x_i}\right), \tag{28}$$

$$v_i(\mathbf{r},t+\Delta t)=v_i(\mathbf{r},t)+\frac{\Delta t}{\rho(\mathbf{r})}\left(\frac{\partial \sigma_{ij}(\mathbf{r},\mathrm{t})}{\partial x_j}+f_i(\mathbf{r},\mathrm{t})\right). \tag{29}$$

(In this section index rather than bold notation will be used, as its greater flexibility will be useful. The unit dyadic $\widehat{\mathbf{k}}\widehat{\mathbf{k}}$ will be written as $\widehat{k}_i\widehat{k}_j$ and the p and s components in this section will be identified with superscripts rather than the subscripts used in Sec. II C above.)

First, a simple overview of the numerical scheme will be given for an initial value problem. Essentially, at each time step the field is split into shear and compressional components so that separate shear and compressional derivative operators can be used on the two components. The two parts of field are then recombined before being separated again at the next timestep. Details of the actual implementation used in the examples, which used staggered time and space grids and absorbing boundaries will be described in more detail below, and the implementation of the sources will be discussed in Sec. III.

Starting with the initial conditions, $\sigma_{ij}(\mathbf{r},t=0)$ and $v_i(\mathbf{r},t=0)$, Eqs. (28) and (29) could be solved numerically using the following sequential scheme:

(1) Separate the particle velocity vector into compressional and shear (p and s) components, $v_i(\mathbf{k},\mathrm{t})=v_i^p(\mathbf{k},\mathrm{t})+v_i^s(\mathbf{k},\mathrm{t})$, using

$$v_i^p(\mathbf{k},\mathrm{t})=\widehat{k}_i\widehat{k}_jv_j(\mathbf{k},\mathrm{t}),\quad v_i^s(\mathbf{k},\mathrm{t})=(\delta_{ij}-\widehat{k}_i\widehat{k}_j)v_j(\mathbf{k},\mathrm{t}). \tag{30}$$

(2) Calculate the particle velocity divergence, $\partial v_k/\partial x_k$, the dyadic, $\partial v_j/\partial x_i$, and its transpose, $\partial v_i/\partial x_j$, by calculating the p and s contributions separately using the p and s k-space gradient operators, from (27),

$$\frac{\partial_{p,s}[\cdot]}{\partial_{x_j}}=F^{-1}\{ik_j\,\mathrm{sinc}(\widehat{c_{p,s}}k\Delta t/2)F\{\cdot\}\}, \tag{31}$$

where, in order to ensure the stability,[31] $\widehat{c_{p,s}}$ is taken as the maximum value of the compressional/shear wave speed in the medium, i.e., $\widehat{c_{p,s}}=\max\left(c_{p,s}(\mathbf{r})\right)$.

(3) Calculate p and s updates to the stress tensor such that

$$\Delta\sigma_{ij}^{p,s}(\mathbf{r},\mathrm{t})=\lambda(\mathbf{r})\delta_{ij}\frac{\partial_{p,s}v_k^{p,s}(\mathbf{r},\mathrm{t})}{\partial x_k}+\mu(\mathbf{r})\left(\frac{\partial_{p,s}v_i^{p,s}(\mathbf{r},\mathrm{t})}{\partial x_j}+\frac{\partial_{p,s}v_j^{p,s}(\mathbf{r},\mathrm{t})}{\partial x_i}\right), \tag{32}$$

$$\sigma_{ij}^{p,s}(\mathbf{r},t+\Delta t)=\sigma_{ij}^{p,s}(\mathbf{r},t)+\Delta t\Delta\sigma_{ij}^{p,s}(\mathbf{r},t). \tag{33}$$

(4) Recombine the shear and compressional components and calculate the velocity vector at the next step

$$\frac{\partial\sigma_{ij}}{\partial x_j}(\mathbf{r},t+\Delta t)=\frac{\partial_p\sigma_{ij}^p(\mathbf{r},t+\Delta t)}{\partial x_j}+\frac{\partial_s\sigma_{ij}^s(\mathbf{r},t+\Delta t)}{\partial x_j}, \tag{34}$$

$$v_i(\mathbf{r},t+\Delta t)=v_i(\mathbf{r},t)+\frac{\Delta t}{\rho(\mathbf{r})}\left(\frac{\partial\sigma_{ij}}{\partial x_j}(\mathbf{r},t+\Delta t)\right). \tag{35}$$

(5) Return to Eq. (30) to start the next timestep.

Note that mode conversion will occur when the material parameters are non-homogeneous so it is necessary to combine and re-separate the velocity field to ensure that this occurs, i.e., the parts of the field that have been converted from shear wave to compressional are reassigned to the compressional part of the field (and vice versa) when it is re-split.

This scheme was implemented using staggered grids and absorbing boundaries, details of which are in the next section.

III. NUMERICAL IMPLEMENTATION

A. Implementation using spatial and temporal staggered grids

Staggered grids have found widespread use in the numerical models of wave propagation, in particular in finite-difference methods because (to give a simple example) the calculation of a central difference estimate of a gradient is more accurate than the corresponding forward or backward difference. In spectral methods this improvement in the gradient calculation is not required, but staggered grids have nevertheless been shown to improve stability and efficiency in pseudospectral methods.[34]

The spatial staggered grid scheme shown in Fig. 1 was used in the examples in Sec. IV. Note that for a two-dimensional implementation only the top layer of the staggered grid shown in Fig. 1 is required. In order to use staggered grids it is necessary to define the material properties on the half-spatial-step grids. Time-staggering was also used: the velocities were calculated at times half a timestep, $\Delta t/2$, different from the stresses.

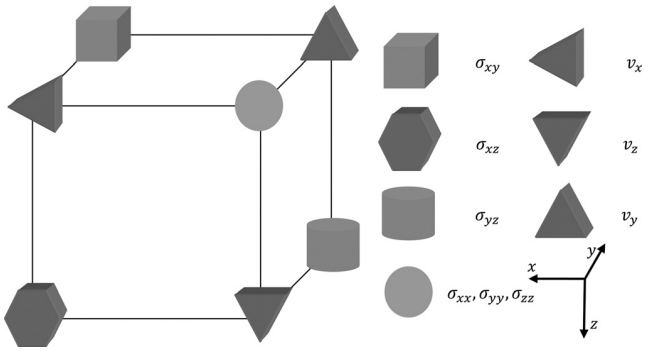

FIG. 1. Three-dimensional spatial staggered grid scheme. In the two-dimensional implementation just the top layer of the staggered grid was implemented. Time-staggering was also used: the stresses were calculated at times $n\Delta t, n = 0, 1, \ldots$, and the velocities at the shifted times $(n + 1/2)\Delta t$.

The calculations of the gradients of the field components at the staggered grid points were calculated by shifting the Fourier components by half a grid spacing as follows [cf. Eq. (31)]:

$$\frac{\partial_{p,s}[\cdot]}{\partial x_j^{\pm}} = F^{-1}\left\{ik_j \text{sinc}\,(\widehat{c_{p,s}}k\Delta t/2)e^{\pm ik_j\Delta x_j/2}F\{\cdot\}\right\}. \tag{36}$$

Using these notations allows the full discrete equations to be written succinctly. The six equations for updating the shear and compressional parts of each of the three velocity components can be written as

$$\begin{aligned} v_i^{p,s}(\mathbf{r}, t + \Delta t/2) = {} & v_i^{p,s}(\mathbf{r}, t - \Delta t/2) \\ & + \frac{\Delta t}{\rho^i(\mathbf{r})}\left\{\frac{\partial_{p,s}\sigma_{ii}^{p,s}(\mathbf{r}, t)}{\partial x_i^+}\right. \\ & \left. + \sum_{j\neq i}\frac{\partial_{p,s}\sigma_{ij}^{p,s}(\mathbf{r}, t)}{\partial x_j^-}\right\}, \end{aligned} \tag{37}$$

where the summation convention is *not* used. The following notation is used above and in Eq. (38): $\rho^x(\mathbf{r}) = \rho(x + \Delta x/2, y, z)$, $\rho^y(\mathbf{r}) = \rho(x, y + \Delta y/2, z)$, $\rho^z(\mathbf{r}) = \rho(x, y, z + \Delta z/2)$, $\mu^{xy}(\mathbf{r}) = \mu(x + \Delta x/2, y + \Delta y/2, z)$, $\mu^{xz}(\mathbf{r}) = \mu(x + \Delta x/2, y, z + \Delta z/2)$, $\mu^{yz}(\mathbf{r}) = \mu(x, y + \Delta y/2, z + \Delta z/2)$ and on the normal grid $\mu(\mathbf{r}) = \mu(x, y, z)$ and $\lambda(\mathbf{r}) = \lambda(x, y, z)$.

The twelve stress components (six stress components split into shear and compressional parts) can be updated using the following equation:

$$\begin{aligned} \sigma_{ij}^{p,s}(\mathbf{r}, t+\Delta t) = {} & \sigma_{ij}^{p,s}(\mathbf{r}, t) + \Delta t\lambda(\mathbf{r})\delta_{ij}\left(\frac{\partial_{p,s}v_k^{p,s}(\mathbf{r}, t+\Delta t/2)}{\partial x_k^-}\right) \\ & + \Delta t 2\mu^*(\mathbf{r})\left(\frac{\partial_{p,s}v_i^{p,s}(\mathbf{r}, t+\Delta t/2)}{\partial x_j^-}\right. \\ & \left. + \frac{\partial_{p,s}v_j^{p,s}(\mathbf{r}, t+\Delta t/2)}{\partial x_i^-}\right), \end{aligned} \tag{38}$$

where $\mu^*(\mathbf{r}) = \mu(\mathbf{r})$ for $i = j$ (normal grid) and $\mu^*(\mathbf{r}) = \mu^{ij}(\mathbf{r})$ for $i \neq j$ (staggered grids), and in this equation the summation convention *is* used. Note when using staggered grids, the wave number domain unit dyadic $(\widehat{k_i}\widehat{k_j})$ must be modified according to Eqs. (39a) and (39b) in order to account for the shifts in medium properties and field variables.

$$(\widehat{k_i}\widehat{k_j})_{\text{staggeredgrids}} = (\widehat{k_i}\widehat{k_j})_{\text{normalgrids}} \times \xi_{ij}, \tag{39a}$$

where ξ_{ij} is as an arbitrary function defined as

$$\xi_{ij} = \begin{cases} 1 & \text{for } i = j \\ e^{i(k_{x_i}\Delta x_i - k_{x_j}\Delta x_j)/2} & \text{for } i \neq j, \end{cases} \tag{39b}$$

where the i before the parentheses is the imaginary number, *not* to be confused with the subscript i. Notable is that the staggered grids unit dyadics is *not symmetric*, in contrary to normal grids unit dyadics.

B. Absorbing boundary condition

The periodicity in the field implied by using discrete Fourier transforms to calculate the spatial gradients results in the wavefield "wrapping"—when a wave leaves one side of the domain it instantly appears on the opposite side. This effect, sometimes referred to as a "periodic boundary condition," means that the computational domain must be larger (perhaps significantly larger) than the domain of interest to avoid contamination of the field of interest by the wrapped field. This would result in a considerable increase in memory requirements, especially in the 3D case, so measures that avoid the wave wrapping are desirable. One approach is to employ a perfectly matched layer (PML) at the edges of the domain which gradually decreases the magnitude of the waves in a strip close to the edge so that by the time they reach the boundary and wrap around, the amplitude of the wrapped field is negligible. However, it is not sufficient just to absorb all of the field components in a strip close to each of the boundaries as this will affect the field in the main (non-PML) part of the domain. This is tackled, for the case of acoustic waves, by artificially dividing the scalar pressure field into subfields associated with each spatial direction[31] so that only the split of the field normal to the boundaries is attenuated in the PML.

Similar PMLs for elastic wave propagation are implemented by writing the field in terms of potentials, then artificially dividing them into direction-dependants splits and attenuating the directional splits normal to the boundaries.[35] The disadvantage of this approach for a Fourier based method is that the potential fields and their dependant auxiliary fields would necessarily be calculated everywhere, due to the nonlocal behavior of the Fourier transform. This would require the introduction of numerous unnecessary variables at each timestep. In an alternative approach used in this paper, the components of the vector and tensor fields themselves are used directly in the implementation of the PML.[36] In order to incorporate this approach into the present k-space method, in a generic three-dimensional problem, the

six components of the velocity field and the twelve components of the stress field (recall that each component has a shear and compressional part) are split into three directions, to allow the x, y, and z splits to be attenuated independently. This increases the number of variables that must be stored, but its greater effectiveness as a PML allows the absorbing region to be reduced in thickness. Three PML absorption coefficients are used to effect this, α_x, α_y, and α_z. This is shown below, suppressing for the moment the temporal staggering. For the velocity fields,

$$\frac{\partial_{p,s}}{\partial t}\left({}_i v_i^{p,s}(\mathbf{r},t)\right) = \alpha_i\left({}_i v_i^{p,s}(\mathbf{r},t)\right) + \frac{1}{\rho^i(\mathbf{r})}\left\{\frac{\partial_{p,s}\sigma_{ii}^{p,s}(\mathbf{r},t)}{\partial x_j^+}\right\}, \tag{40a}$$

$$\frac{\partial_{p,s}}{\partial t}\left({}_j v_i^{p,s}(\mathbf{r},t)\right) = \alpha_j\left({}_j v_i^{p,s}(\mathbf{r},t)\right) + \frac{1}{\rho^i(\mathbf{r})}\left\{\frac{\partial_{p,s}\sigma_{ij}^{p,s}(\mathbf{r},t)}{\partial x_j^-}\right\}, \quad j \neq i. \tag{40b}$$

For the stress fields,

$$\frac{\partial_{p,s}}{\partial t}\left({}_k\sigma_{ii}^{p,s}(\mathbf{r},t)\right) = \alpha_k\left({}_k\sigma_{ii}^{p,s}(\mathbf{r},t)\right) + (\lambda(\mathbf{r}) + \mu(\mathbf{r})\delta_{ki}) \times \left(\frac{\partial_{p,s} v_k^{p,s}(\mathbf{r},t)}{\partial x_k^-}\right), \quad k = x,y,z, \tag{41a}$$

$$\frac{\partial_{p,s}}{\partial t}\left({}_i\sigma_{ij}^{p,s}(\mathbf{r},t)\right) = \alpha_i\left({}_i\sigma_{ij}^{p,s}(\mathbf{r},t)\right) + \mu^{ij}(\mathbf{r})\left(\frac{\partial_{p,s} v_j^{p,s}(\mathbf{r},t)}{\partial x_i^+}\right), \quad j \neq i, \tag{41b}$$

$$\frac{\partial_{p,s}}{\partial t}\left({}_j\sigma_{ij}^{p,s}(\mathbf{r},t)\right) = \alpha_j\left({}_j\sigma_{ij}^{p,s}(\mathbf{r},t)\right) + \mu^{ij}(\mathbf{r})\left(\frac{\partial_{p,s} v_i^{p,s}(\mathbf{r},t)}{\partial x_j^+}\right), \quad j \neq i \tag{41c}$$

where $k,i,j = x,y,z$. Note that the summation convention is *not* used in Eqs. (40a), (40b), (41a), (41b), and (41c). Labeling the artificially direction-dependant splits of each field is based on gradients of that field along each particular spatial direction. To see this, consider the stress field σ_{xx} in the 2D plane (x,y) σ_{xx} is calculated at each timestep as $(\lambda+2\mu)\partial u_x/\partial x + \lambda\partial u_y/\partial y$. The x-part is then referred to be as $(\lambda+2\mu)\partial u_x/\partial x$ (proportional to the gradient along x direction) and the y-part is considered as $\lambda\partial u_y/\partial y$ (proportional to the gradient along y direction).

Following Tabei *et al.*,[31] the equations above are in the form of $\partial R/\partial t = \alpha R + Q$ so can be rearranged as $\partial(e^{\alpha t}R(t))/\partial t = e^{\alpha t}Q(t)$ which is in a form more stable for calculation. The full equations as they were implemented, including the staggered temporal and spatial grids and PML in the above form are given in the Appendix. Here, the absorption coefficients $(\alpha_{x_j}, j = x,y,z)$ are chosen according to a power law attenuation as

$$\alpha_{xj} = \alpha_{max}\frac{c_{max}}{\Delta x_j}\left(\frac{x_j - x_{j0}}{x_{jmax} - x_{j0}}\right)^n, \tag{42}$$

where x_{j0} is the coordinate at the inner edge of the PML, x_{jmax} is the coordinate at the outer edge of the grid, c_{max} is the maximum value of the compressional and shear wave speeds, Δx_j is the grid spacing in the PML, and α_{max} is the maximum absorption in Nepers per cell, within the PML.

C. Source implementation

For the numerical simulations, two types of sources, compressional monopoles and plane waves, were modeled in the two-dimensional space (x,y). For implementation purposes, the source given with profile $f(t)$ is first considered in the form of the displacement compressional potential (ϕ), and then the elasticity constitutive equations [Eqs. (1) and (2)] are applied to calculate the stresses for each timestep; so that a short pulse in ultrasound or its counterpart in seismology and oceanography, an explosive source, can be modeled by adding a known value to stress components, while keeping the initial velocities equal to zero.

Given the source profile as $f(t)$, an incident cylindrical compressional wave may be written as $\phi = f(t - r/c_p)/\sqrt{r}$, where r is the distance from the origin, $r = \sqrt{x^2+y^2}$. This form can be used to model a line source in the 3D space or a monopole source in 2D planes. Using constitutive equations [Eqs. (1) and (2)], we can write,

$$\sigma_{xx} = \rho c_p^2\left\{2g + r\frac{\partial g}{\partial r}\right\} - 2\rho c_s^2\left\{g + \frac{y^2}{r}\frac{\partial g}{\partial r}\right\}, \tag{43a}$$

$$\sigma_{yy} = \rho c_p^2\left\{2g + r\frac{\partial g}{\partial r}\right\} - 2\rho c_s^2\left\{g + \frac{x^2}{r}\frac{\partial g}{\partial r}\right\}, \tag{43b}$$

$$\sigma_{xy} = \rho c_s^2\frac{xy}{r}\frac{\partial g}{\partial r}, \tag{43c}$$

where $g = -(1/2c_p^2 r^2\sqrt{r})\{f(t - r/c_p) + 2\sqrt{r}f'(t - r/c_p)\}$. To fulfill these conditions, one can *equally* add a known value to the normal stresses at the same nodal point, while keeping the shear stress equal to zero. This equivalency has been shown by Refs. 13 and 37. In the 3D space, where a monopole propagates spherical waves in the form of $\phi = f(t - r/c_p)/r$, a similar approach could be undertaken and the same conclusion would be drawn.[38]

A compressional plane wave propagating along an arbitrary direction x_j of a 2D space with an arbitrary time profile $f(t)$ may be written as $f(t - x_j/c_p)$; using constitutive equations in Cartesian coordinates, assuming that the wave propagates in the x direction, we then can write,

$$\sigma_{xx} = \frac{\lambda+2\mu}{c_p^2}f''\left(t - \frac{x}{c_p}\right), \quad \sigma_{yy} = \frac{\lambda}{c_p^2}f''\left(t - \frac{x}{c_p}\right), \quad \sigma_{xy} = 0, \tag{44}$$

where $f'' = \partial^2 f/\partial t^2$. Equations (44) show that including a compressional plane wave source in x direction involves

unequally adding a known value proportional to the Lamé parameters to normal stresses at a line of nodes perpendicular to the direction of propagation while keeping the shear stress equal to zero. Note that in the case of acoustic waves, $\mu = 0$, $\sigma_{xx} = \sigma_{yy} = -P$, where P is the acoustic pressure; therefore, normal stress fields are updated equally. Likewise, similar relations could be written for a plane wave propagating in the 3D space.

In all the following examples, the time profiles of the sources for the normal stresses are considered to be the first and the second derivatives of a Gaussian pulse with the center frequency a and the time delay t_o.

IV. EXAMPLES

A. Monopole in an infinite homogenous medium

As a first example, consider a point source in an unbounded homogenous medium. An explosive source is modeled using the derivative of a Gaussian shape with the center frequency $a = 6.4$ Hz and the time delay $t_o = 0.225$ s (allowing sufficient time before the pulse reaches its peak to ensure that the input pulse is effectively zero at $t = 0$). With a medium with the compressional wave speed of $c_p = 4000\,\mathrm{m\,s^{-1}}$, the shear wave speed of $c_s = 2400\,\mathrm{m\,s^{-1}}$ and the density of $\rho = 2700\,\mathrm{kg\,m^{-3}}$, the number of grid elements is set 150 in each direction with equal grid-spacing of 100 m (which corresponds to only 3 points per minimum wavelength in the medium). The Courant–Friedrichs–Lewy criterion is $\mathrm{CFL} = c_0\Delta t/\Delta x$, where c_0 for elastic waves should be replaced by the maximum of the compressional and shear wave speeds, and was set to 0.3. The receiver is located at 400 m from the source. A PML is used on all the edges of the grid to simulate a two-dimensional unbounded space. For effective attenuation on the edges of the boundary, a PML thickness of 20 grid points, together with a maximum PML absorption coefficient of $\alpha_{max} = 4$ and absorption power of $n = 4$, were empirically found to be sufficient to minimize boundary reflection and wraparound effects.

Figure 2 shows the radial component of the displacement compared with the analytical solution for the case of an infinite (unbounded) homogenous medium, which is obtained by numerically convolving the pulse shape with the Green's function solution given by Ref. 39, which shows excellent agreement. In Fig. 3 the net energy of the propagating elastic wave is plotted versus time to first ensure that the method well-preserves the energy and second demonstrate the effectiveness of the PML by showing how the energy of the propagating wave decreases as a function of time once it reaches the PML. Region (a) corresponds to the time when the source energy is input. Region (b) is the main portion of the simulation in which the wave travels towards the boundaries. As it can be observed, the energy is well-preserved as an important characteristic of a numerical method. Region (c) is when the wavefront reaches the boundary and is being absorbed and finally region (d) is after all the energy is absorbed. For this purpose, the total duration of the simulation was extended to 4 sec to ensure that all the travelling energy is absorbed effectively.

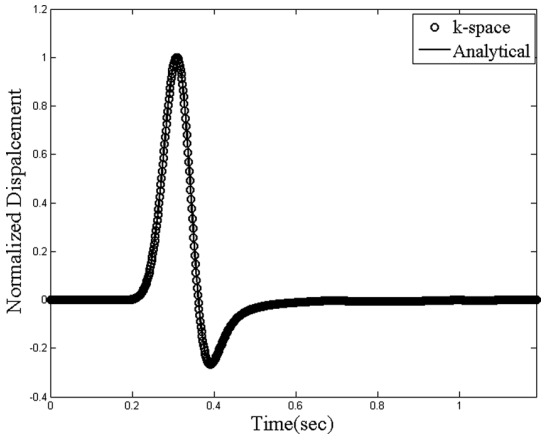

FIG. 2. The radial displacement as a function of time 400 m from an explosive source in a 2D homogenous elastic medium (i.e., cylindrical wave propagation). Analytical solution (solid), *k*-space method (circles).

B. Two homogenous half-spaces

The second example considers an explosive source in a fluid half-space overlying an elastic half-space. The explosive source is modeled as the second derivative of a Gaussian (also known as the Ricker wavelet), with the center frequency $a = 4$ Hz and the initial time delay $t_o = 0.5$s. The acoustic (fluid) region is modeled simply by letting $\mu = 0$, or equivalently, $c_s = 0$. The source is located in the fluid at 870 m above the interface and the receiver is positioned at 870 m above the interface with the horizontal distance of 600 m from the source. The acoustic properties of the fluid are considered as those of water (the sound speed of $c_f = 1500\,\mathrm{m\,s^{-1}}$ and the density of $\rho = 1000\,\mathrm{kg\,m^{-3}}$) and the elastic region is considered as soil with the compressional wave speed of $c_p = 3400\,\mathrm{m\,s^{-1}}$, the shear wave speed of $c_s = 2500\,\mathrm{m\,s^{-1}}$ and the density of $\rho = 1963\,\mathrm{kg\,m^{-3}}$. The PML is set as in the previous example.

In order to demonstrate the accuracy, the velocity components time series for the recorded signal at the receiver are compared with the analytical solution. In order to obtain the analytical solution, the Green's function given by Ref. 40, for acoustic wave reflection from a solid-fluid flat interface,

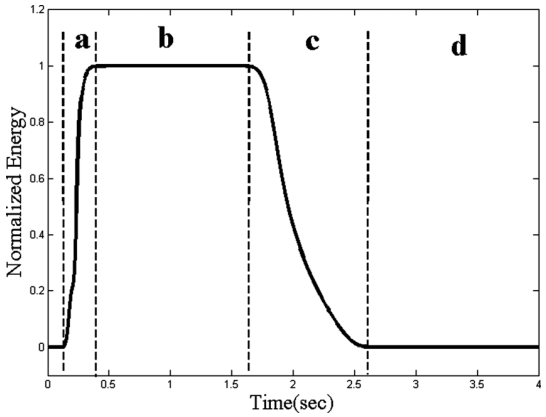

FIG. 3. The net energy of the propagating wave vs time. After the source is added to the field [region (a)], the energy is preserved [region (b)] until the wave reaches the PML [region (c)], where it is attenuated, after which gradually there is no energy remaining in the domain [region (d)].

is convolved numerically with the time-profile of the source, using the code obtained from Ref. 41. The number of grid nodes is 400 (to allow the wavefronts evolve sufficiently to capture all types of the waves as discussed below) in each direction with equal grid spacing of 15 m, which corresponds to 8 points per minimum wavelengths (PPMW). Figure 4 shows the comparison of the results of the *k*-space method and the analytical solution for CFL = 0.25, which shows excellent agreement.

First, in order to assess the temporal accuracy and stability, the method is compared with the staggered leapfrog pseudospectral (PSTD) method, in which the time integration is implemented using the classical finite differencing. For this purpose, the CFL number (which in essence is representing the size of the timestep) was varied from 0.1 up to 1.4 to measure the accuracy of each of the schemes. The efficiency of the *k*-space approach becomes apparent when the L_2 error of the time series is plotted versus various choices of CFL for both the *k*-space and the staggered leapfrog methods. This is shown in Fig. 5. It is not surprising that for small timesteps, both numerical methods are accurate, but once a larger CFL is chosen, the leapfrog PSTD becomes inaccurate and eventually unstable. Note that the L_2 errors for the leapfrog PSTD method are not given for the CFL numbers above 0.5 because the computation becomes severely unstable for higher CFL numbers while, the *k*-space method remains stable. The error of the *k*-space method does increase as the timestep increases, but much more slowly.

In the second step, the spatial accuracy of the method is also verified by making comparisons with the second and fourth-order finite difference time domain (FDTD) schemes[13,14] of the same model problem (i.e., stress-velocity formulation) of elastodynamics. The codes for this purpose were obtained from Ref. 42. The error of each method was evaluated against the analytical solution for different points per minimum wavelengths (from 2 up to 15). To realize this, the grid spacing was varied accordingly from 60 m to 8 m and the CFL number was set to 0.2 to ensure a sufficient temporal accuracy for each of the methods. Figure 6 shows the trend of the L_2 error versus the choices of the PPMW. As evident, even compared with the fourth-order FDTD, the *k*-space method has a major improvement in accuracy for the same PPMW, up to about 7 PPMW. Of course, for large PPMW all the methods converge to the exact solution but as far as the computational efficiency is concerned, the *k*-space method can result in significant reduction in the computational effort for a same degree of accuracy, especially in large scale problems.

For completeness, a snapshot of propagation of the absolute value of the velocity field is also presented in Fig. 7 in the dB scale. Several wavefronts are clearly distinguishable. These waves are labeled as "a," Direct Wave; "b," Reflected Wave; "c," Head Wave; "d," Transmitted Compressional Wave; and "e," Transmitted Shear Wave.

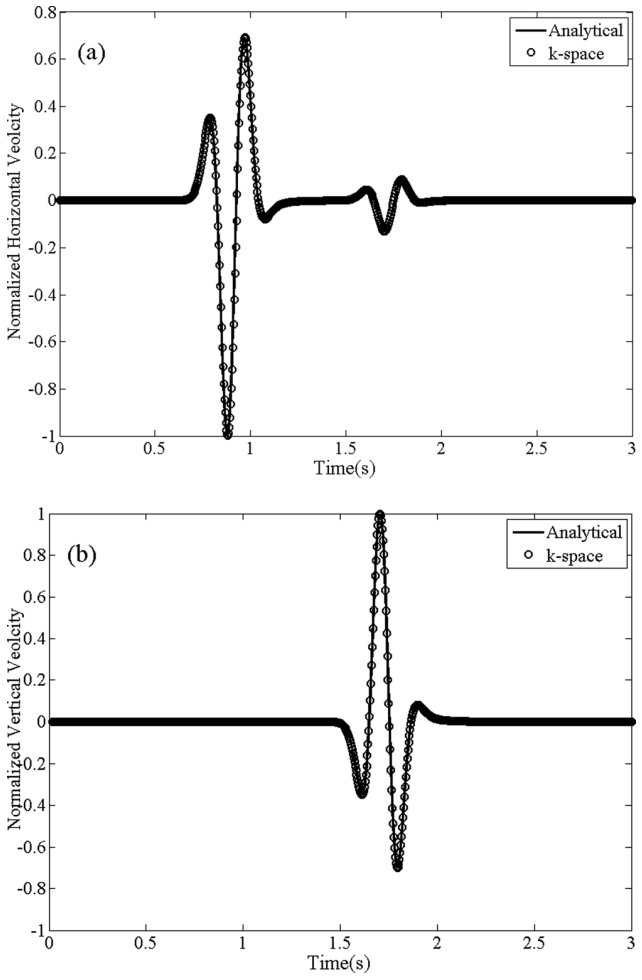

FIG. 4. Velocity components time-series at the receiver for the example of an explosive source above a fluid-solid interface (Sec. IV B). Analytical solution (solid), *k*-space method (circles). (a) Horizontal particle velocity. (b) Vertical particle velocity.

C. Heterogeneous medium: Scattering of plane waves by cylindrical inclusions

An example of scattering of compressional plane waves by a cylindrical inclusion is modeled. In this example, the

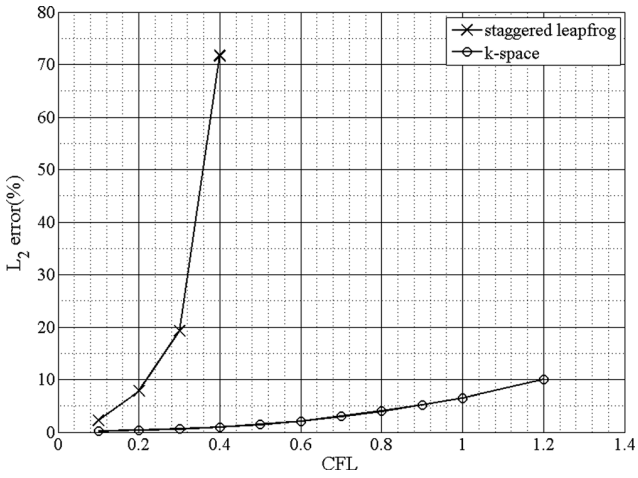

FIG. 5. Comparison of accuracy of the *k*-space method and the staggered leapfrog pseudospectral method: L_2 error of the "measured" time series as a function of CFL number.

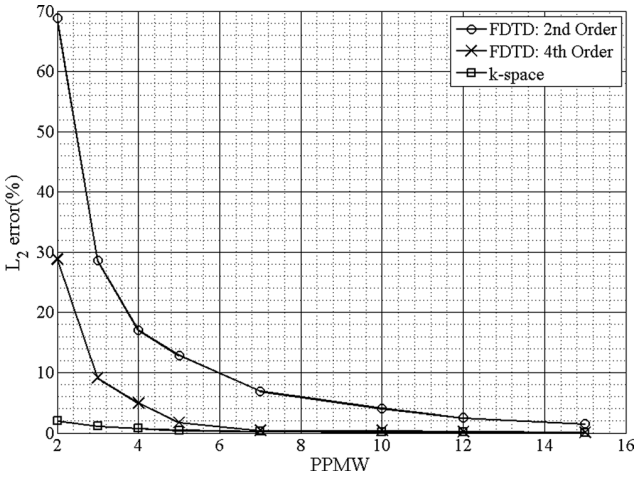

FIG. 6. Comparison of accuracy of the *k*-space method and the 2nd and 4th order FDTD methods: L_2 error of the "measured" time series as a function of PPMW number.

scattering of elastic waves from an elastic cylindrical fiber is modeled and the results are compared with the analytical solution. The cylindrical inclusion is a Silicon Carbide fiber imbedded in a Titanium alloy matrix, which is a composite material of interest in aerospace applications. The properties of the matrix are given as $c_p = 4500\,\mathrm{m\,s^{-1}}$, $c_s = 2000\,\mathrm{m\,s^{-1}}$ and $\rho = 4800\,\mathrm{kg\,m^{-3}}$ and the fiber as $c_p = 10\,000\,\mathrm{m\,s^{-1}}$, $c_s = 4100\,\mathrm{m\,s^{-1}}$ and $\rho = 2800\,\mathrm{kg\,m^{-3}}$. The excitation is a pulsed plane wave with the time profile of the derivative of a Gaussian, with the center frequency $a = 5$ MHz and the time delay $t_o = 300$ ns. The adjustments of the PML are similar to the previous examples; however, to efficiently model a plane wave propagating along the horizontal direction, the PML is switched off on the top and bottom edges of the domain. This is necessary to avoid the diffraction resulting from the two end nodes of the line of source points, therefore to create a plane wave consistent with the theoretical definition of pulsed plane waves. However, in the stimulation of plane wave scattering from cylindrical inclusions, since periodic boundary conditions have been used, the duration of the simulation is limited to the time when the points being monitored have not been contaminated by the wrapped wave field. In the example shown here it has been ensured that the results are not affected by this limitation. The number of grid nodes is 256 in each direction with equal grid spacing of 50 μm (this corresponds to 9 points per minimum wavelength in the medium). The CFL is considered as 0.25

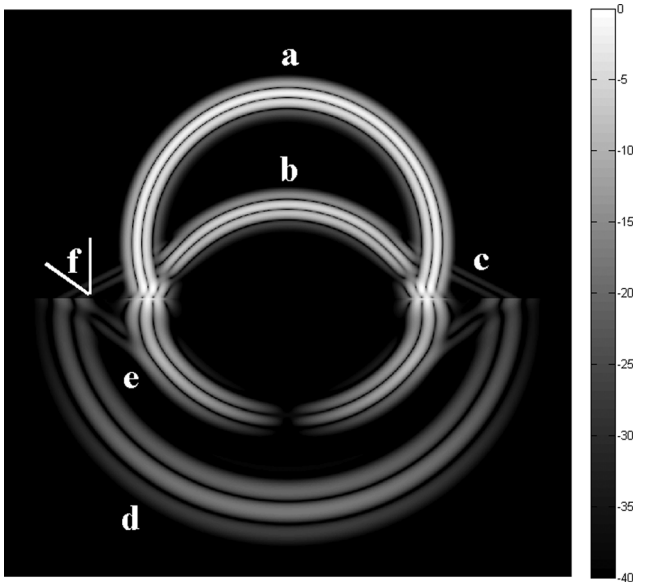

FIG. 7. Snapshot of the absolute value of the velocity field in the dB scale at time t = 1.47 s for the example in Fig. 4. Various wavetypes are clearly distinguishable: (a) direct and (b) reflected P-waves in the fluid, (c) head waves, (d) transmitted P waves in the solid, and (e) S-waves (converted from P-waves) in the solid. (f) Demonstrates the critical angle.

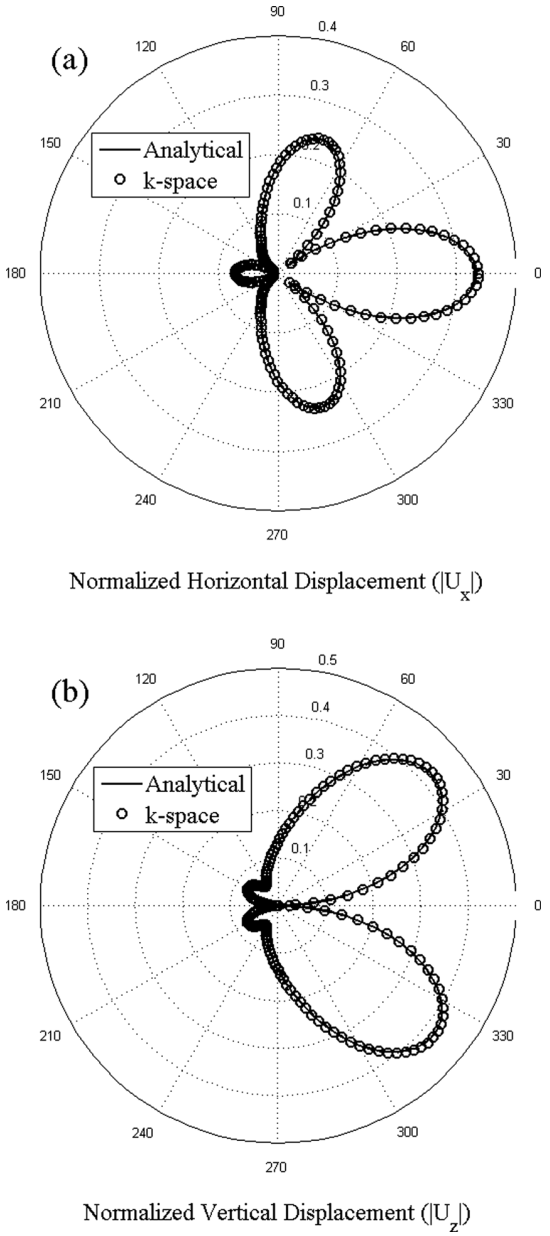

FIG. 8. Amplitude of the (a) horizontal and (b) vertical displacements at a distance of 3a (where a is the radius of the scatterer) at 5 MHz. Analytical solution (solid), *k*-space method (circles).

for a satisfactory degree of accuracy. The radius of the scatterer in is assumed to be 1.2 mm.

The comparisons of the frequency domain analytical solution given by Ref. 43 and the numerical results for both the vertical and the horizontal displacements are presented in Fig. 8. In order to obtain the numerical results in the frequency domain, a broad band pulse was used, and the scattered field at $r = 3.6$ mm was transformed to the frequency domain. The results were then compared for an arbitrary frequency of 500 kHz, and show excellent agreement. Snapshots of propagation of the wavefronts for the net velocity amplitude are presented in Fig. 9 in the dB scale.

This example shows that the presented *k*-space method can conveniently handle scattering problems of interest in several fields, and can result in significant efficiency gains compared to other methods such as FD, especially when the scattering effects of complex geometries are to be investigated. This is of interest in many different applications, including ultrasonic Non-Destructive Evaluation (NDE) of inhomogeneous materials with complex microstructure, ultrasound scattering from solid particles in colloidal systems, seismology, geophysics and biomedical engineering.

V. DISCUSSION

The *k*-space model presented here for elastic waves can be significantly more efficient than conventional finite element and FD methods, and even pseudo-spectral models. Like PSTD models, the *k*-space method describes the high-frequency elastic waves in a Fourier basis so requires fewer mesh points per wavelength than FD methods. However, the use of the *k*-space adjustment permits larger time steps without reducing accuracy

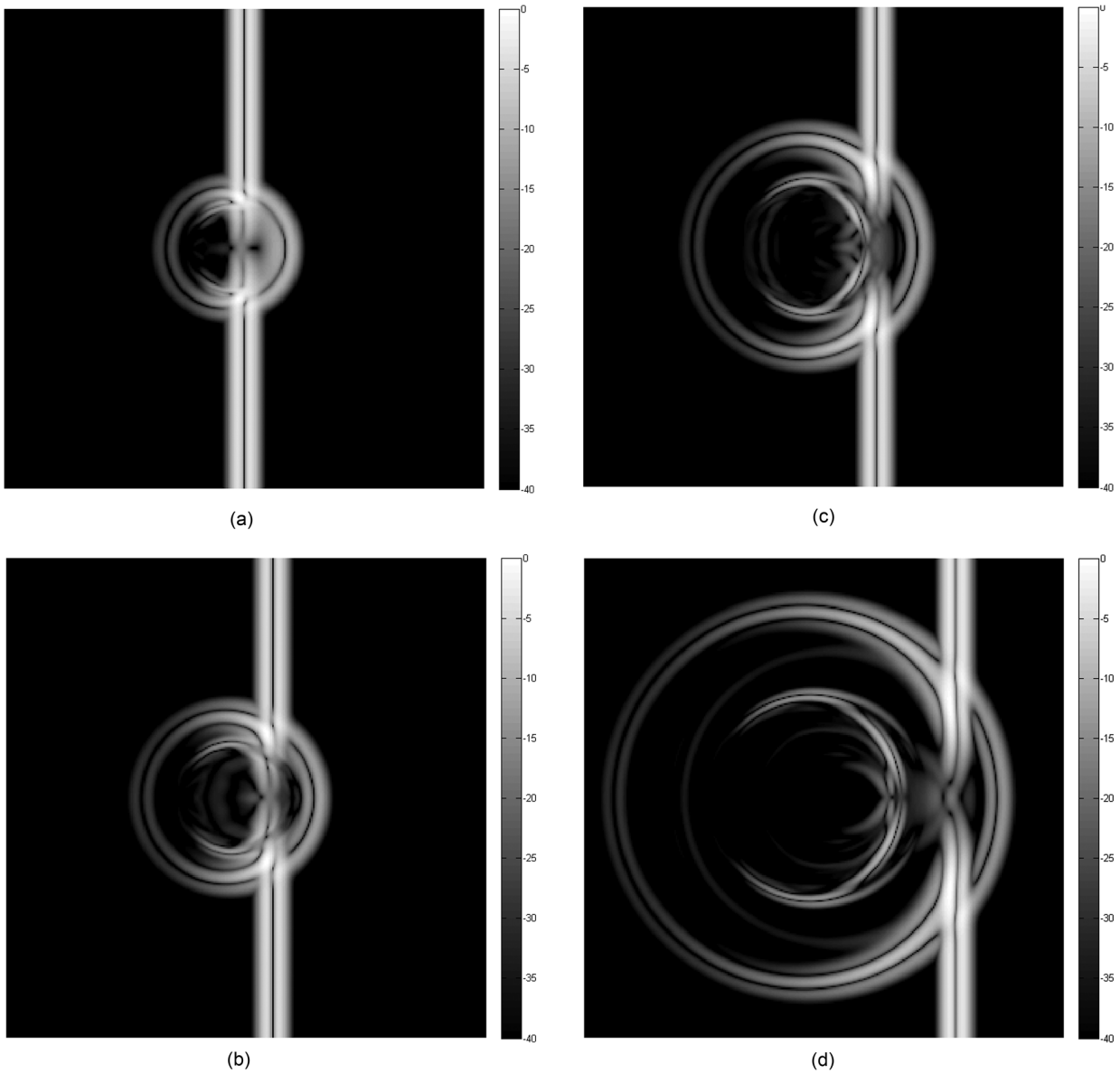

FIG. 9. Snapshots of absolute value velocity field in the dB scale for the example of scattering of a pulsed plane wave by a single elastic cylindrical fiber imbedded in an elastic matrix (Sec. IV C) at times t = 1.31, 1.5, 1.7 and 2.25 μs (the incident plane wave is propagating from left to right).

or introducing instability. The method maintains the advantages of the previous acoustic and elastic *k*-space methods; like those, the present method is temporally and spatially exact for homogeneous media, and spectrally accurate in space for smoothly varying heterogeneous media. In practice, it is still useful for modeling non-smooth media, although in such cases more than two PPW are typically required.

When the heterogeneous elastic wave equation [Eq. (7)] is re-written in the form of the stress-velocity formulation [Eqs. (5) and (6)], the spatial derivatives of the medium properties (i.e., density, and compressional and shear wave speeds) are eliminated. In such cases, first order operators are applied for the spectral calculation of the spatial derivatives of the field variables. In comparison with Liu's second order *k*-space approach,[30] both methods essentially have the same accuracy for homogenous media since they are mathematically identical. On the one hand, Liu's method requires computation and storage of only the displacement fields, while the present method requires computation and storage of the stresses as well as the velocity components. However, the first order *k*-space method has the capability of conveniently incorporating PML absorbing boundary conditions. For large computations, the high performance of the PML allows the grid size to be substantially reduced without introduction of wraparound or boundary-reflection errors, so that the present *k*-space method can often perform more efficiently, especially in three-dimensional problems.

The developed *k*-space method could also be thought of as a modified leapfrog pseudospectral (PSTD) method for the stress-velocity formulation of elastodynamics. The modification is via introducing two temporal propagators, each of which is associated with propagation of one mode. In leapfrog pseudospectral methods, although the first order spatial derivatives are accurately calculated using the fast Fourier transform (FFT), for higher degrees of accuracy schemes such as Adams–Bashforth iteration are commonly required.[44,45] The temporal correction provided by the *k*-space method eliminates the need for higher-order time schemes. However, the previous studies have shown that the pseudospectral methods employing fourth-order Adams-Bashforth time integration shows trends similar to that of PSTD in Fig. 5.[46,47]

The other advantages of this method are (a) the ability of being used for modeling the acoustic medium by simply letting the shear speed be zero, and more importantly, (b) the capability of efficiently and accurately modeling interactions of elastic and fluid media with significant savings in computations compared to other approaches such as Virieux's stress-velocity FD method.[13] For highly heterogeneous media, where discontinuities exist in medium properties, numerical artifacts (Gibbs phenomena) may arise from applying FFTs. The resulting inaccuracies could be minimized by smoothing the media using an appropriate smoothing algorithm such as a spatial-frequency domain Hanning window.

VI. SUMMARY

A new *k*-space method for numerical modeling of elastic waves, using the first order stress-velocity formulation, has been described. The exact second order *k*-space solution has been derived for homogenous media, and then, the leapfrog pseudospectral scheme for time integration has been modified with the *k*-space second order operators, which makes time integration more stable. The *k*-space second order operators, when decomposed into first order operators were applied to discretize the stress-velocity equations for modeling elastic wave propagation in heterogeneous media. Staggered spatial and temporal grids were used. The step by step formulation of the method when incorporating the staggered grids has been described and a new model that can incorporate perfectly matched layers (PMLs) as the absorbing boundary conditions has been explained. For validation of the method, examples of propagation of elastic waves in homogenous and heterogeneous media have been compared with the analytical solutions and the results have been discussed with regards to the accuracy and efficiency of the method. Further examples have been given to show the efficiency and flexibility of the method when applied to large scale scattering problems.

APPENDIX

To avoid confusion with the use of subscripts when developing the full 3D relations of the *k*-space method by using Eqs. (37) and (38) combined with the PML [Eqs. (40) and (41)], the full development is presented here for arbitrary selections of velocity and stress components in the three-dimensional space. As each field is subdivided into compressional and shear wave splits, the following development is represented for both by using superscripts. As an example of the velocity fields, v_x is presented; σ_{xx} and σ_{xy} are fully developed as examples of the stress tensor field. Denoting $x^+ = x + \Delta x/2$, $y^+ = y + \Delta y/2$, $z^+ = z + \Delta z/2$, $t^+ = t + \Delta t/2$, $t^- = t - \Delta t/2$, and $t^{++} = t + \Delta t$,

(1) Velocity field (v_x):

$$
\begin{aligned}
&{}_x v_x^{p,s}(x^+, y, z, t^+) \\
&\quad = e^{\alpha_x \Delta t/2} \Bigg\{ e^{\alpha_x \Delta t/2}\, {}_x v_x^{p,s}(x^+, y, z, t^-) \\
&\qquad + \frac{\Delta t}{\rho(x^+, y, z)} \left(\frac{\partial_{p,s} \sigma_{xx}^{p,s}(x, y, z, t)}{\partial x^+} \right) \Bigg\},
\end{aligned}
$$

$$
\begin{aligned}
&{}_y v_x^{p,s}(x^+, y, z, t^+) \\
&\quad = e^{\alpha_y \Delta t/2} \Bigg\{ e^{\alpha_y \Delta t/2}\, {}_y v_x^{p,s}(x^+, y, z, t^-) \\
&\qquad + \frac{\Delta t}{\rho(x^+, y, z)} \left(\frac{\partial_{p,s} \sigma_{xy}^{p,s}(x^+, y^+, z, t)}{\partial y^-} \right) \Bigg\},
\end{aligned}
$$

$$
\begin{aligned}
&{}_z v_x^{p,s}(x^+, y, z, t^+) \\
&\quad = e^{\alpha_z \Delta t/2} \Bigg\{ e^{\alpha_z \Delta t/2}\, {}_z v_x^{p,s}(x^+, y, z, t^-) \\
&\qquad + \frac{\Delta t}{\rho(x^+, y, z)} \left(\frac{\partial_{p,s} \sigma_{xz}^{p,s}(x^+, y, z^+, t)}{\partial z^-} \right) \Bigg\},
\end{aligned}
$$

$$v_x = {}_x v_x^p + {}_y v_x^p + {}_z v_x^p + {}_x v_x^s + {}_y v_x^s + {}_z v_x^s.$$

(2) Normal stress field (σ_{xx}):

$$ {}_x\sigma_{xx}^{p,s}(x,y,z,t^{++}) = e^{\alpha_x \Delta t/2}\left\{ e^{\alpha_x \Delta t/2}\, {}_x\sigma_{xx}^{p,s}(x,y,z,t) + \Delta t[\lambda(x,y,z)+2\mu(x,y,z)] \times \left(\frac{\partial_{p,s} v_x^{p,s}\left(x^+,y,z,t^+\right)}{\partial x^-} \right) \right\},$$

$$ {}_y\sigma_{xx}^{p,s}(x,y,z,t^{++}) = e^{\alpha_y \Delta t/2}\left\{ e^{\alpha_y \Delta t/2}\, {}_y\sigma_{xx}^{p,s}(x,y,z,t) + \Delta t\lambda(x,y,z) \times \left(\frac{\partial_{p,s} v_y^{p,s}\left(x,y^+,z,t^+\right)}{\partial y^-} \right) \right\},$$

$$ {}_z\sigma_{xx}^{p,s}(x,y,z,t^{++}) = e^{\alpha_z \Delta t/2}\left\{ e^{\alpha_z \Delta t/2}\, {}_z\sigma_{xx}^{p,s}(x,y,z,t) + \Delta t\lambda(x,y,z) \times \left(\frac{\partial_{p,s} v_z^{p,s}\left(x,y,z^+,t^+\right)}{\partial z^-} \right) \right\},$$

$$\sigma_{xx} = {}_x\sigma_{xx}^p + {}_y\sigma_{xx}^p + {}_z\sigma_{xx}^p + {}_x\sigma_{xx}^s + {}_y\sigma_{xx}^s + {}_z\sigma_{xx}^s.$$

(3) Shear Stress field (σ_{xy}):

$$ {}_x\sigma_{xy}^{p,s}(x^+,y^+,z,t^{++}) = e^{\alpha_x \Delta t/2}\left\{ e^{\alpha_x \Delta t/2}\, {}_x\sigma_{xy}^{p,s}(x^+,y^+,z,t) + \Delta t\mu(x^+,y^+,z) \times \left(\frac{\partial_{p,s} v_y^{p,s}\left(x,y^+,z,t^+\right)}{\partial x^+} \right) \right\},$$

$$ {}_y\sigma_{xy}^{p,s}(x^+,y^+,z,t^{++}) = e^{\alpha_y \Delta t/2}\left\{ e^{\alpha_y \Delta t/2}\, {}_y\sigma_{xy}^{p,s}(x^+,y^+,z,t) + \Delta t\mu(x^+,y^+,z) \times \left(\frac{\partial_{p,s} v_x^{p,s}\left(x^+,y,z,t^+\right)}{\partial y^+} \right) \right\},$$

$$\sigma_{xy} = {}_x\sigma_{xy}^p + {}_y\sigma_{xy}^p + {}_x\sigma_{xy}^s + {}_y\sigma_{xy}^s \quad {}_z\sigma_{xy}^p = {}_z\sigma_{xy}^s = 0.$$

Other field components, velocities v_y and v_z, and stresses σ_{yy}, σ_{zz}, σ_{xz}, and σ_{yz} could be developed in a similar manner.

[1] H. Sato and M. C. Fehler, *Seismic Wave Propagation and Scattering in the Heterogeneous Earth*, 1st ed. (Springer, Berlin, 2009), 308 pp.
[2] J. Carcione, *Waves and Fields in Real Media: Wave Propagation in Anisotropic, Anelastic, and Porous Media* (Handbook of Geophysical Exploration, Seismic Exploration Series) (Pergamon, Amsterdam, 2001), Vol. 31, 538 pp.
[3] A. Leger and M. Deschamps (Eds.), *Ultrasonic Wave Propagation in Non Homogeneous Media* (Springer Proceedings in Physics) (Springer, Berlin, 2009), Vol. 128, 435 pp.
[4] B. Luthi, *Physical Acoustics in the Solid State* (Springer, Berlin, 2005), 420 pp.
[5] J. D. Cheeke, *Fundamentals and Applications of Ultrasonic Waves* (CRC Press, London, 2002), 480 pp.
[6] A. Arnau Vives, *Piezoelectric Transducers and Applications*, 2nd ed. (Springer, Berlin, 2008), 532 pp.
[7] E. Bossy, M. Talmant, and P. Laugier, "Three-dimensional simulations of ultrasonic axial transmission velocity measurement on cortical bone models," J. Acoust. Soc. Am. **115**(5), 2314–24 (2004).
[8] W. D. Smith, "The application of finite element analysis to body wave propagation problems," Geophys. J. R. Astron. Soc. **42**(2), 747–768 (1975).
[9] F. J. Rizzo, D. J. Shippy, and M. Rezayat, "A boundary integral equation method for radiation and scattering of elastic waves in three dimensions," Int. J. Numer. Meth. Eng. **21**(1), 115–129 (1985).
[10] E. Dormy and A. Tarantola, "Numerical simulation of elastic wave propagation using a finite volume method," J. Geophys. Res. **100**(B2), 2123–2133 (1995).
[11] R. J. Leveque, *Finite Volume Methods for Hyperbolic Problems* (Cambridge Texts in Applied Mathematics Series, No. 31) (Cambridge University Press, Cambridge, UK, 2002), 578 pp.
[12] W. C. Chew, M. S. Tong, and B. Hu, "Integral equation methods for electromagnetic and elastic waves," *Synthesis Lectures on Computational Electromagnetic*, No. 12 (Morgan and Claypool Publishers, San Rafael, CA, 2009), 241 pp.
[13] J. Virieux, "P-SV wave propagation in heterogeneous media: Velocity-stress finite-difference method," Geophysics **51**(4), 889–901 (1986).
[14] A. Levander, "Fourth-order finite-difference P-SV seismograms," Geophysics **53**(11), 1425–1436 (1988).
[15] P. Moczo, J. O. A. Robertsson, and L. Eisner, "The finite-difference time-domain method for modeling of seismic wave propagation," Adv. Geophys. **48**, 421–516 (2007).
[16] D. D. Kosloff and E. Baysal, "Forward modeling by a Fourier method," Geophysics **47**, 1402–1412 (1982).
[17] B. Fornberg, "The pseudospectral method: Comparisons with finite differences for the elastic wave equation," Geophysics **52**(4), 483–501 (1987).
[18] B. Fornberg, "The pseudospectral method: Accurate representation of interfaces in elastic wave calculations," Geophysics **53**(5), 625–637 (1988).
[19] D. Gottlieb and J. S. Hesthaven, "Spectral methods for hyperbolic problems," J. Comp. Appl. Math. **128**(1–2), 83–131 (2001).
[20] J. S. Hesthaven, S. Gottlieb, and D. Gottlieb, *Spectral Methods for Time-Dependent Problems* (Cambridge Monographs on Applied and Computational Mathematics Series, No. 21) (Cambridge University Press, New York, 2007), 284 pp.
[21] C. G. Canuto, M. Y. Hussaini, A. Quarteroni, and T. A. Zang, *Spectral Methods: Fundamentals in Single Domains* (Springer, Berlin, 2006), 581 pp.
[22] B. Fornberg, *A Practical Guide to Pseudospectral Methods* (Cambridge Monographs on Applied and Computational Mathematics Series, No. 1) (Cambridge University Press, New York, 1998), 244 pp.
[23] B. Fornberg and G. B. Whitham, "A numerical and theoretical study of certain nonlinear wave phenomena" Philos. Trans. R. Soc. London A **289**(1361), 373–404 (1978).
[24] N. N. Bojarski, "The k-space formulation of the scattering problem in the time domain," J. Acoust. Soc. Am. **72**(2), 570–584 (1982).
[25] N. N. Bojarski, "The k-space formulation of the scattering problem in the time domain: An improved single propagator formulation," J. Acoust. Soc. Am. **77**(3), 826–831 (1985).
[26] B. Compani-Tabrizi, "k-space scattering formulation of the absorptive full fluid elastic scalar wave equation in the time domain," J. Acoust. Soc. Am. **79**(4), 901–905 (1986).
[27] S. Finette, "Computational methods for simulating ultrasonic scattering in soft tissue," IEEE Trans. Ultrason., Ferroelectr., Freq. Control **34**(3), 283–292 (1987).

[28]S. Finette, "A computer model of acoustic wave scattering in soft tissue," IEEE Trans. Biomed. Eng. **34**(5), 336–344 (1987).
[29]S. Pourjavid and O. J. Tretiak, "Numerical solution of the direct scattering problem through the transformed acoustical wave equation," J. Acoust. Soc. Am. **91**(2), 639–645 (1992).
[30]Q. H. Liu, "Generalisation of the k-space formulation to elastodynamic scattering problems," J. Acoust. Soc. Am. **97**(3), 1373–1379 (1995).
[31]M. Tabei, T. D. Mast, and R. C. Waag, "A k-space method for coupled first-order acoustic propagation equations," J. Acoust. Soc. Am. **111**(1), 53–63 (2002).
[32]B. T. Cox, S. Kara, S. R. Arridge, and P. C. Beard, "k-space propagation models for acoustically heterogeneous media: Application to biomedical photoacoustics," J. Acoust. Soc. Am. **121**(6), 3453–3464 (2007).
[33]B. E. Treeby and B. T. Cox, "k-Wave: MATLAB toolbox for the simulation and reconstruction of photoacoustic wave fields," J. Biomed. Optics **15**(2), 021314 (2010).
[34]B. Fornberg, "High-order finite differences and the pseudospectral method on staggered grids," SIAM J. Numer. Anal. **27**(4), 904–918 (1990).
[35]F. D. Hastings, J. B. Schneider, and S. L. Broschat, "Application of the perfectly matched layer (PML) absorbing boundary condition to elastic wave propagation," J. Acoust. Soc. Am. **100**(5), 3061–3069 (1996).
[36]W. C. Chew and Q. H. Liu, "Perfectly matched layers for elastodynamics: A new absorbing boundary condition," J. Comp. Acoust. **4**, 341–359 (1996).
[37]Z. Alterman and F. C. Karal, "Propagation of elastic waves in layered media by finite-difference methods," Bull. Seism. Soc. Am. **58**(1), 367–398 (1968).
[38]Y. Q. Zeng and Q. Liu, "A multidomain PSTD method for 3D elastic wave equations," Bull. Seismol. Soc. Am. **94**(3), 1002–1015 (2004).
[39]E. Kausel, *Fundamental Solutions in Elastodynamics: A Compendium* (Cambridge University Press, New York, 2006), 260 pp.
[40]A. T. de Hoop, "A modification of Cagniard's method for solving seismic pulse problems," Appl. Sci. Res. B **8**, 349–356 (1960).
[41]http://www.spice-rtn.org/library/software/EX2DELEL.html (Last viewed April 10, 2012).
[42]https://www.geoazur.net/PERSO/operto/HTML/fwm2dpsv.html (Last viewed April 10, 2012).
[43]C. C. Mow and Y. H. Pao, "The diffraction of elastic waves and dynamic stress concentrations" (RAND Corporation, Santa Monica, CA, 1971), 696 pp.
[44]M. Ghrist, B. Fornberg, and T. A. Driscoll, "Staggered time integrators for wave equations," SIAM J. Numer. Anal. **38**(3), 718–741 (2000).
[45]O. Bou Matar, V. Preobrazhensky, and P. Pernod, "Two-dimensional axisymmetric numerical simulation of supercritical phase conjugation of ultrasound in active solid media," J. Acoust. Soc. Am. **118**(5), 2880–2890 (2005).
[46]G. Wojcik, B. Fornberg, R. Waag, L. Carcione, J. Mould, L. Nikodym, and T. Driscoll, "Pseudospectral methods for large-scale bioacoustic models," Proc. IEEE Ultrason. Symp. **2**, 1501–1506 (1997).
[47]J. C. Mould, G. L. Wojcik, L. M. Carcione, M. Tabei, T. D. Mast, and R. C. Waag, "Validation of FFT-based algorithms for large-scale modeling of wave propagation in tissue," Proc. IEEE Ultrason. Symp. **2**, 1551–1556 (1999).